Controlling vortex breakdown in swirling pipe flows: Experiments and simulations

D. J. C. Dennis, C. Seraudie, and R. J. Poole

Citation: Physics of Fluids (1994-present) **26**, 053602 (2014); doi: 10.1063/1.4875486
View online: http://dx.doi.org/10.1063/1.4875486
View Table of Contents: http://scitation.aip.org/content/aip/journal/pof2/26/5?ver=pdfcov
Published by the AIP Publishing

This article is copyrighted as indicated in the article. Reuse of AIP content is subject to the terms at: http://scitation.aip.org/termsconditions. Downloaded to IP: 138.253.116.83 On: Thu, 08 May 2014 13:20:35

PHYSICS OF FLUIDS **26**, 053602 (2014)

Controlling vortex breakdown in swirling pipe flows: Experiments and simulations

D. J. C. Dennis,[1,a)] C. Seraudie,[2] and R. J. Poole[1]
[1]*School of Engineering, University of Liverpool, Liverpool L69 3GH, United Kingdom*
[2]*Ecole Centrale de Nantes, 1, rue de la No. B.P. 92101, 44321 Nantes Cedex 3, France*

(Received 18 February 2014; accepted 28 April 2014; published online 8 May 2014)

A laminar, incompressible, viscous pipe flow with a controllable swirl induced by wall rotation has been studied both numerically and experimentally up to an axial Reynolds number (*Re*) of 30. The pipe consists of two smoothly joined sections that can be rotated independently about the same axis. The circumstances of flow entering a stationary pipe from a rotating pipe (so-called decaying swirl) and flow entering a rotating pipe from a stationary pipe (growing swirl) have been investigated. Flow visualisations show that at a certain swirl ratio the flow undergoes a reversal and vortex breakdown occurs. The variation of this critical swirl ratio with Reynolds number is explored and good agreement is found between the experimental and numerical methods. At high *Re* the critical swirl ratio tends to a constant value, whereas at low *Re* the product of the Reynolds number and the square of the swirl ratio tends to a constant value in good agreement with an existing analytical solution. For decaying swirl the vortex breakdown manifests itself on the pipe axis, whereas for growing swirl a toroidal zone of recirculation occurs near the pipe wall. The recirculating flow zones formed at critical conditions are found to increase radially and axially in extent with increasing Reynolds number and swirl ratio. © *2014 AIP Publishing LLC*. [http://dx.doi.org/10.1063/1.4875486]

I. INTRODUCTION

Vortex breakdown of swirling flows – the formation of a stagnation point upstream of a region of near-stagnant recirculating flow – has fascinated and intrigued many since its discovery nearly 60 years ago.[1–4] One of the key reasons for such continued study is surely the inherent artistic beauty embedded within it (coupled with the non-trivial fluid dynamics at play). Classic flow visualisation text books[5] contain numerous such examples: experiments[6] and numerical simulations[7] of vortex breakdown in a rotating endwall cylindrical container; experiments[5] and numerical simulations[8] of vortex breakdown on delta wings. Other examples of such visualisations can be found in papers studying cylindrical divergent tubes[9,10] and slit-tube arrangements[11] amongst many other flows.

In the current paper we revisit a set-up originally proposed by Lavan *et al.*[12] where swirling flow in a constant-diameter cylindrical pipe was considered. In this set-up, the pipe consists of two smoothly joined sections that can be rotated independently about the same axis. Lavan *et al.*[12] combined a linearised analytical solution with a finite-difference numerical technique to probe two cases; that of upstream pipe rotation and downstream pipe stationary which they referred to as *decaying swirl* (a convention we will adhere to in the current paper) and the opposite situation which they called *growing swirl*. In the case of decaying swirl, vortex breakdown was seen to occur on the pipe axis (much as is observed in the cylindrical divergent tubes discussed above) however in the growing-swirl case vortex breakdown occurred at the tube wall and a toroidal zone of recirculation was predicted.

[a)]Electronic mail: David.Dennis@liverpool.ac.uk

 © 2014 AIP Publishing LLC

This article is copyrighted as indicated in the article. Reuse of AIP content is subject to the terms at: http://scitation.aip.org/termsconditions. Downloaded to IP: 138.253.116.83 On: Thu, 08 May 2014 13:20:35

TABLE I. Previous studies of vortex breakdown in swirling pipe flow and conditions studied.

Author and year	Methodology	Decaying swirl cases studied (Re, Γ)	Growing swirl cases studied (Re, Γ)	Conclusions
Lavan *et al.* (1969)[12]	Analytical ($Re \leq 1$) and numerical (finite difference of vorticity/stream-function formulation)	(4.0, 11.97); (4.0, 15); (20, 7.92)	(1.0, 7.95); (20, 5.22); (40, 4.74)	For $Re < 1$: $Re\Gamma^2 =$ constant (512 for decaying; 146 for growing). For $Re \gg 1$: $\Gamma =$ constant ($\approx$8 for decaying; $\approx$5 for growing)
Crane and Burley (1976)[15]	Numerical (finite difference of vorticity/stream-function formulation)	(0.1, 50); (0.2, 35); (0.5, 25); (2.0, 15); (5, 9); (10, 8)		
Silvester *et al.* (1984)[16]	Numerical (finite elements of primitive variable formulation)	(2.0, 20); (4.0, 20); (8.0, 20); (16.0, 20); (4.0, 15); (8.0, 15); (16.0, 15); (8.0, 10); (16.0, 10)		Minor disagreements with Lavan *et al.*[12] noted
Macdonald (1991)[13]	Analytical			For $Re < 1$: $Re\Gamma^2 =$ constant (512.82 for decaying)

The linearisation of Lavan *et al.*[12] was achieved by assuming that the difference between the speeds of rotation of the two ducts is not large relative to the mean rotational speed and that the axial Reynolds number ($Re = UD/\nu$, where U is the bulk velocity, D is the pipe diameter, and ν is the kinematic viscosity) approaches zero while the product of the swirl ratio ($\Gamma = 0.5\omega D/U$ where $0.5\omega D$ is the tangential velocity at the pipe wall) squared and the Reynolds number remains finite (i.e., $Re\Gamma^2 \neq 0$). For an interesting discussion of this solution and its underlying assumptions the reader is directed to Ref. 13.

For Reynolds numbers below about 1, Lavan *et al.*[12] found excellent agreement between the analytical and numerical results and the product of the critical swirl ratio squared and the Reynolds number was found to be constant (albeit a different constant value in the case of decaying ($Re\Gamma^2 = 512$) or growing swirl ($Re\Gamma^2 = 146$)). At larger Reynolds number this scaling broke down and the critical swirl number tended to constant values ($\Gamma \approx 8$ for decaying and $\Gamma \approx 5$ for growing). Thus the location and structure of vortex breakdown can be controlled by the choice of wall rotation in this simple arrangement.

Rusak and Meder[14] conducted an asymptotic analysis of swirling flow in a pipe close to critical conditions. Their analysis showed that wall-separation could be induced by a small, but finite, pipe contraction, which had the effect of accelerating the flow near the axis and decelerating the flow near the wall. This effect could occur below the critical swirl for vortex breakdown and in fact the two mechanisms competed against each other with the wall-separation delaying the onset of vortex breakdown.

Although both the analytical and numerical components of Lavan *et al.*[12] have been revisited and essentially confirmed by Macdonald[13] and Crane and Burley[15]/Silvester *et al.*,[16] respectively, quite remarkably this flow has never been probed experimentally despite its relative simplicity. The precise conditions studied by these four papers are provided in Table I. In addition, as noted by Leibovich, Lavan *et al.* "devote little attention to the structure of the recirculation zone."[2] Therefore, the aim of the current paper is to address these deficits by describing the development and commissioning of a new experimental facility to test this hypothesis of vortex breakdown switching location and to investigate the structure of the recirculating zones. We support experimental dye-injection and reflective anisotropic particle flow visualisations with a detailed numerical investigation.

II. EXPERIMENTAL ARRANGEMENT

The experimental rig used to perform all the experiments in this work is shown schematically in Figure 1. It consists of two identical glass pipes with an internal diameter $D = 50$ mm that are aligned

This article is copyrighted as indicated in the article. Reuse of AIP content is subject to the terms at: http://scitation.aip.org/termsconditions. Downloaded to IP: 138.253.116.83 On: Thu, 08 May 2014 13:20:35

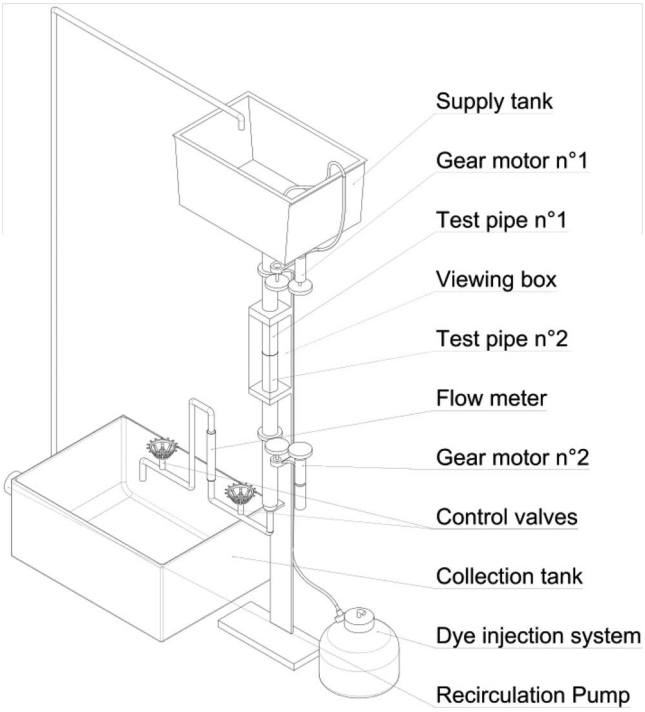

FIG. 1. Schematic of rotating pipe flow facility.

end-on in a vertical orientation. Each of the two pipes is 13D in length. At the junction between the pipes there is a small gap ($<$1 mm) through which the working fluid slowly fills a glass viewing box when the facility is first filled. Once the glass box is filled the mass flow rate through the gap is negligible compared to the flow through the test pipe working section. The viewing box removes distortion due to the curvature of the pipe wall for the purposes of imaging the flow visualisation. The small gap between the two pipes that make up the working section enables the two pipes to be rotated independently using two motors that deliver mechanical power directly to the pipes through a series of 1:1 gears. Motor controllers enable the regulation of the rotational speed of each pipe to an accuracy of ± 2 rpm, with a maximum rotation rate of 400 rpm, providing access to a wide range of swirl ratios (the exact range depends on axial Reynolds number).

The flow is gravity-driven from a supply tank situated at the top of the system. This system approximates to a constant head tank as the volume of fluid and surface area of the tank are large compared to the flow rate through the test pipes. In principle the flow could be recirculated to keep the volume in the supply tank constant by pumping fluid up from the collection tank. In reality this pumping was found to disturb the flow to an undesirable extent during an experiment. This pump was therefore only used to refill the supply tank once the fluid level became low. A honeycomb mesh was installed at the inlet to the upper test pipe to reduce inlet swirl and produce a uniform flow at entry to the first pipe. To control the throughput, two needle valves are located downstream of the working section with a mass flow meter installed between them to monitor the flow rate.

Approximately 40 l of fluid is required to fill the system. All the results presented here have been achieved with a mix of approximately 80% glycerine and 20% water. The glycerine is required to lower the Reynolds number (by increasing the viscosity) into the range where the swirl number achievable with the rotational speed provided by the motors is high enough to cause breakdown. No assumptions were made regarding the properties of the working fluid. The density and temperature were measured before and after each set of experiments using an Anton Paar DMA 35N density meter (with a quoted accuracy of 0.001 g/cm^3 and 0.2 °C). For reference, the density of the mixture was around 1220 kg/m^3. Similarly, the viscosity of the mixture was measured using a TA Instruments Rheolyst AR 1000 N controlled-stress rheometer in conjunction with a 60 mm diameter 2° acrylic

This article is copyrighted as indicated in the article. Reuse of AIP content is subject to the terms at: http://scitation.aip.org/termsconditions. Downloaded to IP: 138.253.116.83 On: Thu, 08 May 2014 13:20:35

cone to within an uncertainty of 2%.[17] The viscosity varied considerably with temperature, which was accounted for as far as possible. For reference, the viscosity of the mixture was approximately 0.13 Pa s at 15 °C, 0.10 Pa s at 20 °C, and 0.07 Pa s at 25 °C.

The flow meter installed on the rotating pipe facility was calibrated for water by the manufacturer of the meter. Consequently, it was necessary to recalibrate for the glycerine-water mix. Recalibration was achieved by timing the period required to fill a measuring cylinder of known volume across the full range of flow rates achievable in the facility. Tese data were used to construct a function (4th order polynomial) to convert from the readings taken directly from the flow meter to the actual flow rate.

Two methods of flow visualisation were employed to observe the vortex breakdown. A dye injection system was used to inject blue dye (food colouring) at the inlet to the pipe (through the honeycomb mesh). The dye was diluted using the working fluid such that the density and viscosity of the resulting fluid were in essence identical to the clear working fluid. The dyed fluid was contained in a separate pressure vessel connected to a controllable supply of compressed air. The dye is delivered by first pressurising the vessel and utilising this pressure to force the dye through narrow plastic tubing leading to a needle positioned in the centre of the pipe at inlet. A needle valve was installed on the delivery tubing to control the flow of dye, which was found to be an important aspect of achieving high-quality visualisations. The dye injection method was found to work well for decaying swirl (upper pipe rotating) as the breakdown in that configuration occurred on the centreline of the pipe, so the dye entered and recirculated in the breakdown bubble. However, the technique was less successful for visualising growing swirl (lower pipe rotating) because the breakdown occurred at the pipe wall, where there was no dye. Moving the dye injection point to near the wall showed an indication of the breakdown, but was still considered unsatisfactory as the internal structure of the bubble was not visualised.

In order to visualise the growing swirl breakdown the flow was seeded with a small quantity of Mearlmaid particles (Engelhard Mearlmaid AA). These particles are anisotropic, highly reflective, flat platelets that tend to align with the shear. They were illuminated using a laser sheet (using a GreenLyte 532 nm 5 mW laser and a cylindrical lens) in the axial-radial plane of the pipe in the region where vortex breakdown was expected to occur. All images, for both types of visualisation techniques, were captured using a Nikon D5200 Digital SLR Camera (24.1 mega-pixel CMOS sensor) equipped with a NIKKOR 18-55 mm lens.

III. NUMERICAL METHOD

To compute the flow field within the rotating pipe flow, discussed above, we make use of the fact that the flow is laminar, incompressible, steady, and axisymmetric (i.e., two-dimensional). The governing equations are then those expressing conservation of mass (Eq. (1)) and momentum (Eq. (2)):

$$\nabla \cdot \boldsymbol{u} = 0, \tag{1}$$

$$\rho\left(\frac{\partial \boldsymbol{u}}{\partial t} + \boldsymbol{u} \cdot \nabla \boldsymbol{u}\right) = -\nabla p + \eta \nabla \cdot \nabla \boldsymbol{u}. \tag{2}$$

In these equations, $\boldsymbol{u}$ represents the vector velocity, p the static pressure, ρ the fluid density, and η its dynamic viscosity. The appropriate boundary conditions for this problem are axisymmetric conditions on the centreline, fixed velocity conditions on the pipe walls, uniform flow velocity at the inlet far upstream of the junction, and the outlet boundary condition far downstream of the junction. To ensure fully developed flow at the junction, the length of each pipe (i.e., upstream and downstream of join) was set to 50 pipe radii: we confirmed this was sufficient[18] for all of the results shown here, where Re is always less than 30, to be independent of this length. We used the commercial package FLUENT (in ANSYS WorkBench 14.5) to solve Eqs. (1) and (2) subject to these boundary conditions. This well-established code has been used extensively in the calculation of

This article is copyrighted as indicated in the article. Reuse of AIP content is subject to the terms at: http://scitation.aip.org/termsconditions. Downloaded to IP: 138.253.116.83 On: Thu, 08 May 2014 13:20:35

TABLE II. Mesh characteristics together with estimates of numerical accuracy for a representative case $Re = 10$, $\Gamma = 15$. Ni = number of cells in the radial ($i = r$) and axial ($i = x$) direction. fi = cell compression ratio in radial ($i = r$) and axial ($i = x$) direction. NC = number of cells.

Mesh	Nr	fr	Nx	fx	NC	X_S	% error in X_S
M1	20	1	800	6.25	16 000	2.444	0.45
M2	40	1	1600	6.25	64 000	2.436	0.13
M3	80	1	3200	6.25	256 000	2.434	0.04
Richardson extrapolation						2.433	

complex flows and, with the correct implementation, is adequate to model the swirling laminar flows under consideration here.[19] We used the segregated solver in which the momentum and swirl velocity equations were discretised using a second-order up-winding scheme. Some limited calculations were also carried out using a theoretically third-order QUICK-type scheme for the convective terms to ascertain the effect of discretisation scheme on the accuracy of our results: the differences were essentially negligible. Coupling of the pressure and velocity was achieved using the well-known SIMPLEC implementation.[20]

Double precision (14 d.p.) was used for all the calculations so that round-off errors are negligible. The iterations were stopped whenever the scaled residuals for the solutions for the two components of velocity and the continuity equation approached an asymptotic value, in general the scaled residuals were observed to reach a level between 1×10^{-12} and 1×10^{-15}.

A preliminary series of calculations was carried out with 20×800, 40×1600, and 80×3200 cells of uniform size in the radial direction and non-uniform in the axial direction for a particular case, well beyond critical conditions, to investigate the accuracy of our simulations ($Re = 10$, $\Gamma = 15$). The details of these meshes are provided in Table II. Our consistent mesh refinement allows us to undertake a quantitative validation and to directly estimate the numerical accuracy of our simulations. A sensitive criterion to determine this accuracy is the axial extent of the vortex breakdown, non-dimensionalised by the pipe radius, which we choose here to define as X_S. The variation of this quantity with increasing mesh refinement for a typical simulation ($Re = 10$, $\Gamma = 15$) is also shown in Table II. First we note that the variation of X_S between meshes is about 0.41% at most and so can be regarded as negligibly small. Second, fitting these points to an equation of the form $a(\Delta r)^p + b$ allows us to estimate the order of accuracy (p) of our simulations.[21] Although our simulations are nominally second order in accuracy, we note that in fact the X_S quantity only converges somewhere between first and second order ($p = 1.54$) probably as a consequence of the linear interpolation involved in its determination. However, if we use this order to estimate the "Richardson" extrapolation value for this quantity (i.e., the value extrapolated to zero mesh size), shown below in Table II, we still find that the error in our simulations is negligibly small. On the basis of this analysis of the mesh dependency, all subsequent calculations were carried out with a 80×3200 mesh (i.e., 256 000 cells).

IV. RESULTS AND DISCUSSION

A. Decaying swirl

An illustrative example of vortex breakdown occurring due to decaying swirl is shown in Figure 2, where $Re = 8$ and $\Gamma = 15$. On the left hand side of Figure 2 is the experimental flow visualisation using dye injection at the centreline of the pipe. A recirculation bubble is clearly visible centred on the pipe axis. For clarity, it is noted that fluid is pumped upstream in the centre of the bubble and downstream around the edges of the bubble. The sense of recirculation can be most easily observed in the movie accompanying the article (Figure 3) (Multimedia view). For this Reynolds number/swirl ratio combination it can be seen that the centre of the vortex is slightly below the join at a streamwise location which corresponds to the widest point of the bubble. This was found to be common for the majority of situations studied. However, at very low Reynolds numbers

This article is copyrighted as indicated in the article. Reuse of AIP content is subject to the terms at: http://scitation.aip.org/termsconditions. Downloaded to IP: 138.253.116.83 On: Thu, 08 May 2014 13:20:35

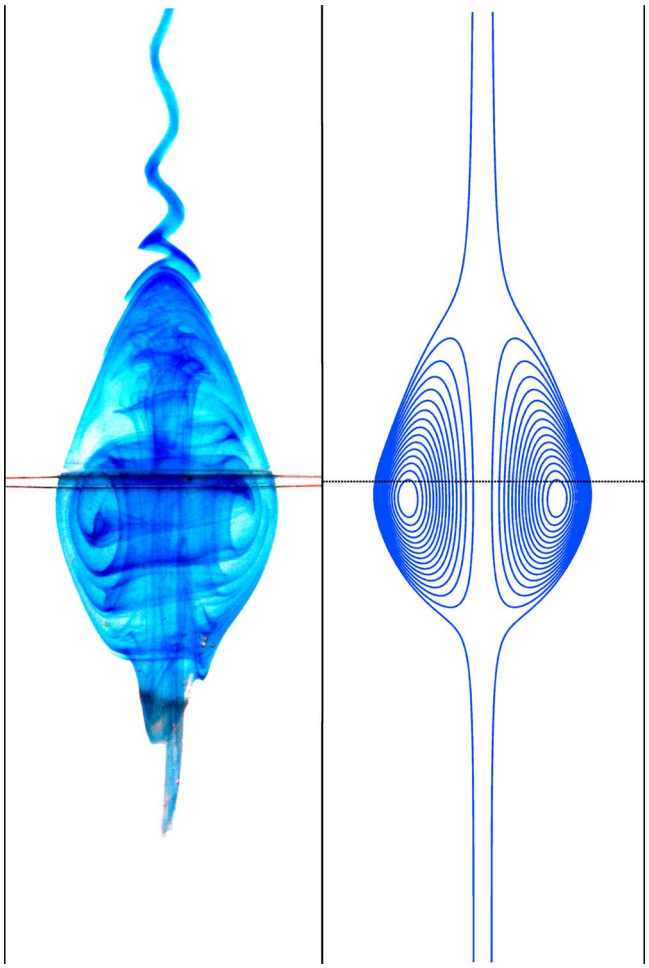

FIG. 2. An illustrative example of vortex breakdown for decaying swirl (upstream pipe rotation) $Re = 8$, $\Gamma = 15$; left hand side experiment; right hand side simulation.

($Re < 4$) it was found that the centre of the recirculation moved upstream of the pipe join at moderate to high swirl ratios ($\Gamma > 15$). On the right hand side of Figure 2 the streamlines from the equivalent axisymmetric numerical simulation have been presented. The similarity in the flow pattern indicated by the experimental visualisation and these streamlines is striking. The bubble is very similar in size and shape, and the centre of recirculation is slightly below the pipe join.

It is notable that the recirculation bubble in Figure 2 ($Re = 8$, $\Gamma = 15$) has a similar length upstream and downstream of the pipe join. (However, the bubble is clearly not symmetrical as the characteristic shape of the bubble is significantly more bulbous downstream of the join of the pipe in comparison to the more pointed shape upstream.) At the same Reynolds number but somewhat higher swirl ratio ($Re = 8$, $\Gamma = 20$), shown in Figure 4, it is noticeable that not only has the bubble increased in size, but that the upstream and downstream lengths of the bubble are no longer similar in extent and the bubble has grown significantly more in the upstream direction. The bubble has also increased in width. However, the centre of the recirculation has not noticeably moved and is still slightly below the join of the pipes.

Figure 5 shows the variation of upstream and downstream extents of the recirculation bubble for a variety of Reynolds number/swirl ratio combinations. Both experimental and numerical results have been included, along with the numerical results of Silvester *et al.*[16] The extent of the recirculation bubble has a precise definition: the region between the two stagnation points. It can therefore be easily extracted from the numerical results. The flow visualisations from the experiment do not provide

This article is copyrighted as indicated in the article. Reuse of AIP content is subject to the terms at: http://scitation.aip.org/termsconditions. Downloaded to IP: 138.253.116.83 On: Thu, 08 May 2014 13:20:35

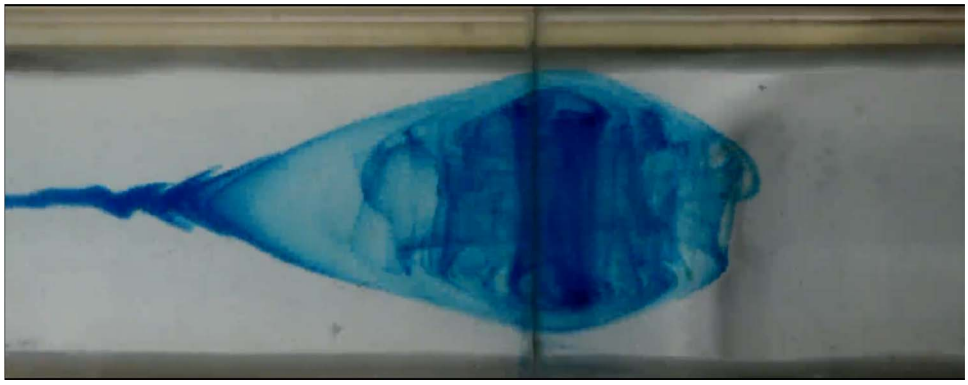

FIG. 3. A movie showing the vortex breakdown for decaying swirl (upstream pipe rotation) $Re = 8$ with gradually increasing and subsequently decreasing swirl ratio; flow is from left to right. (Multimedia view) [URL: http://dx.doi.org/10.1063/1.4875486.1]

this quantitative information and there is some inherent subjectivity in the definition of the extent of the bubble based on viewing the dye injection visualisations alone. The downstream extent of the bubble is particularly difficult to pinpoint in many cases (as highlighted in Figures 2 and 4). However, despite this deficiency, the agreement between the numerical and experimental results in Figure 5

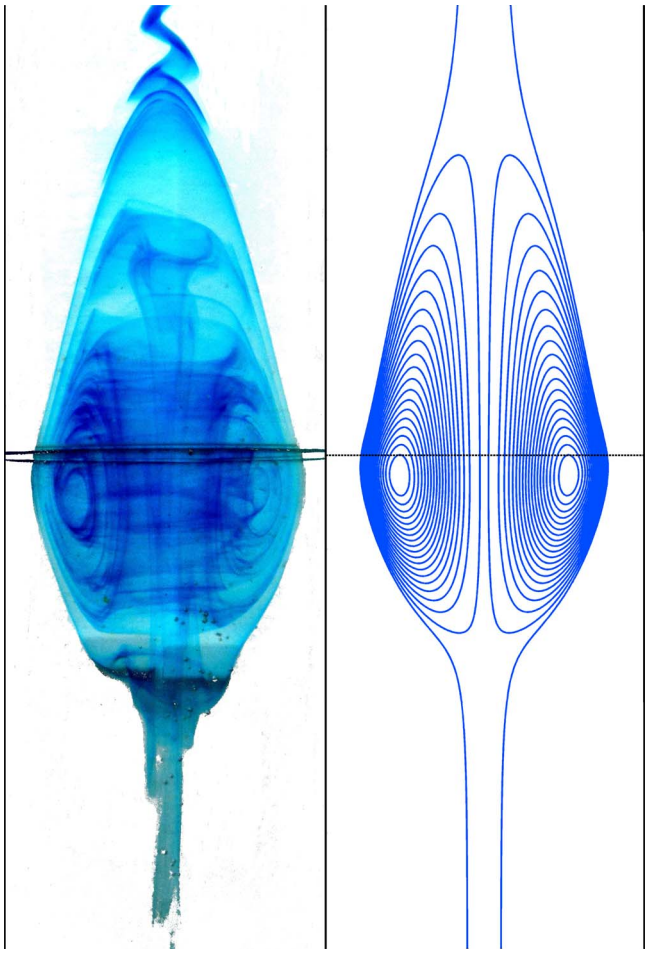

FIG. 4. An illustrative example of vortex breakdown for decaying swirl (upstream pipe rotation) $Re = 8$, $\Gamma = 20$; left hand side experiment; right hand side simulation.

This article is copyrighted as indicated in the article. Reuse of AIP content is subject to the terms at: http://scitation.aip.org/termsconditions. Downloaded to IP: 138.253.116.83 On: Thu, 08 May 2014 13:20:35

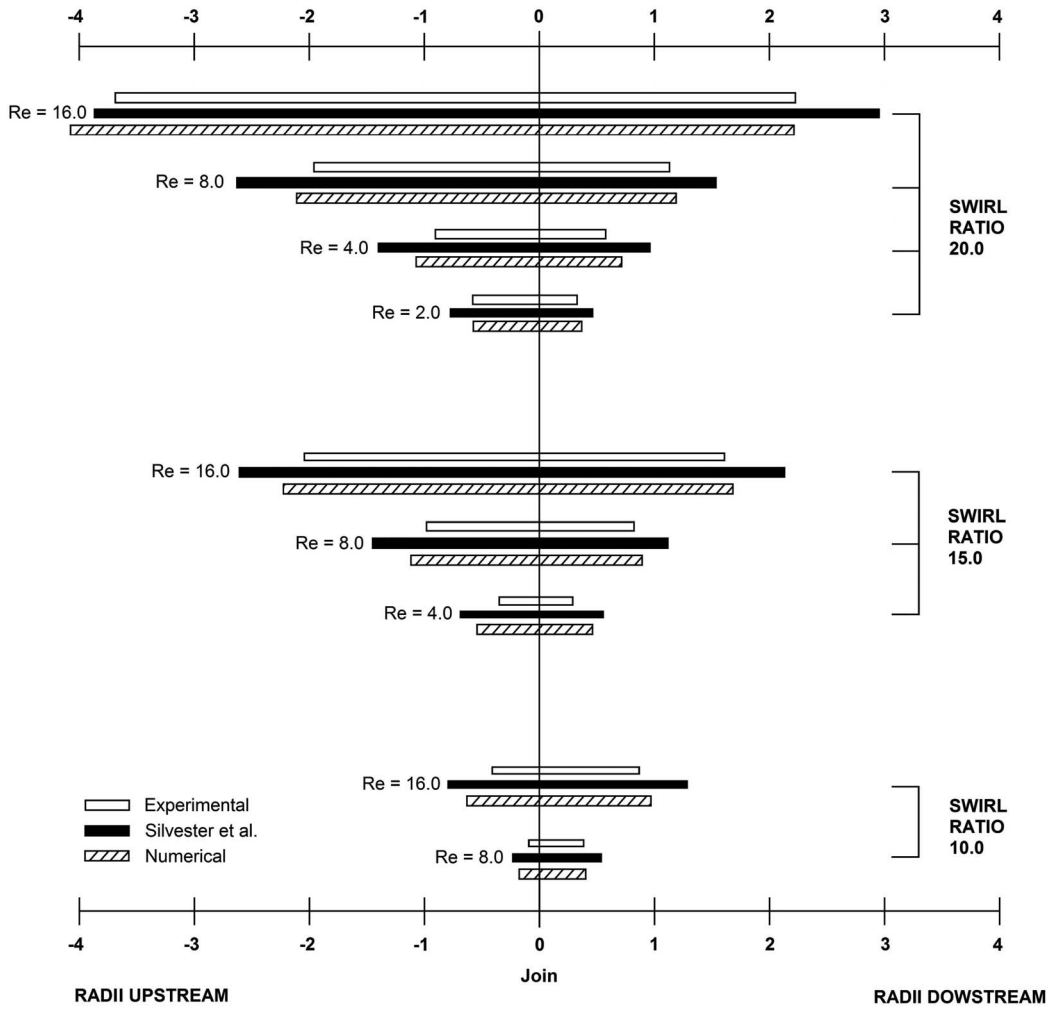

FIG. 5. The variation in upstream and downstream extent of the recirculation bubble for a selection of $Re - \Gamma$ combinations. Including experimental and numerical results from the present study alongside the results from Silvester *et al.*[16]

is very good. In fact the largest discrepancy is found to be in the results of Silvester *et al.*,[16] which consistently overestimate the size of the bubble in the majority of cases. This is thought to be due to possible numerical diffusion due to insufficient resolution in their results (which is understandable given the era of the simulations). It is worth noting that the experimental lengths were measured before any bubble lengths were calculated from our simulations. This removed the possibility of the authors subconsciously exploiting the subjectivity of the experimental measurements in order to match the lengths.

From Figure 5 it is apparent that the length of the recirculation bubble grows with both increasing Reynolds number and increasing swirl ratio. In particular, increasing the swirl ratio favours increasing the bubble length in the upstream direction (although it is increased in the downstream direction also). Increasing the Reynolds number increases the bubble length in both upstream and downstream directions to a similar extent.

B. Critical swirl ratio for vortex breakdown

Figure 6 shows the critical swirl ratio (Γ_c) corresponding to a range of Reynolds number from 2 to 40. The critical swirl ratio is defined as the lowest swirl ratio that causes a stagnation point to occur in the flow at the given *Re* (i.e., the minimum swirl ratio required to induce vortex breakdown).

This article is copyrighted as indicated in the article. Reuse of AIP content is subject to the terms at: http://scitation.aip.org/termsconditions. Downloaded to IP: 138.253.116.83 On: Thu, 08 May 2014 13:20:35

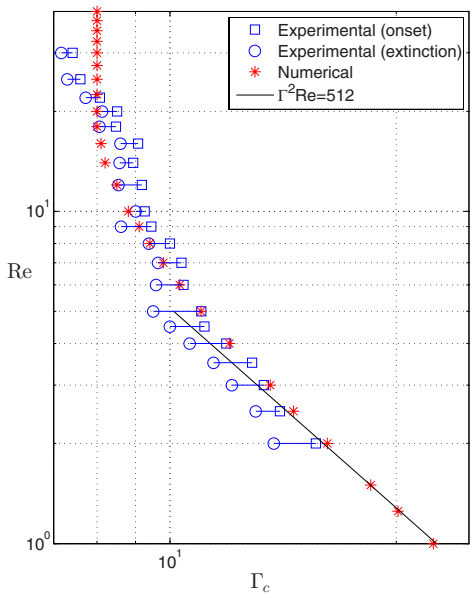

FIG. 6. Stability boundaries for onset of vortex breakdown for decaying swirl (upstream pipe rotation). Solid black line represents analytical results of Lavan *et al.*[12] Red asterisks are the numerical simulations of the current study and the blue symbols are from experimental flow visualisations. Note that both axes are logarithmic.

This definition is the same as that used by Lavan *et al.*[12] Figure 6 shows numerical, analytical, and experimental results. The numerical results clearly demonstrate that at low Re the onset of vortex breakdown is determined by the product of the Reynolds number and the square of the swirl ratio ($\Gamma^2 Re$). Once this parameter exceeds a certain value (found to be 512) vortex breakdown will occur (i.e., at low Re, $\Gamma_c^2 Re = 512$): in agreement with the analytical linearized solution of Lavan *et al.*[12] At higher Reynolds numbers ($Re > 2$) the accuracy of the analytical solution deteriorates. This divergence is perhaps to be expected as the linearization involved in deriving the analytical solution includes the assumption that $Re \to 0$ (but that the product $\Gamma_c^2 Re = 512$ remains finite[12]). For high Reynolds numbers the numerical results show that the critical swirl ratio tends to a constant value, such that for $Re > 20$, $\Gamma_c = 8$.

Figure 6 also includes experimental results that indicate the critical swirl ratio (Γ_c) observed using the dye injection flow visualisation. Here we have included Γ_c for both what we have chosen to call onset and extinction at each Re. These terms indicate when vortex breakdown is first observed as the swirl ratio is increased (onset) and when vortex breakdown disappears as the swirl ratio is decreased (extinction). The rationale for including the two Γ_c is to provide an indication of the uncertainty associated with the task of observing vortex breakdown using dye injection, it is not to suggest that there is a true hysteretic effect (the numerical simulations do not indicate any hysteresis in the critical conditions or dependence on the initial conditions). To exactly match the numerical results we would need to pinpoint the exact Γ when the stagnation point first appears, which is difficult using this qualitative technique. Despite the difficulties associated with this technique the agreement between the experiment and simulation is quite reasonable.

C. Growing swirl

In Figure 7 we present (on the left hand side) a flow visualisation of vortex breakdown caused by growing swirl using illumination of anisotropic particles with a laser sheet ($Re = 8$, $\Gamma = 20$). The flow pattern is quite different from the decaying-swirl case as the recirculation bubble is located at the pipe wall rather than on the pipe axis. This bubble is toroidal in shape with significant elongation in the axial direction, particularly downstream of the pipe join. The main flow (outside of the bubble) is accelerated through the centre rather like a Venturi tube. The right hand side of Figure 7 shows

This article is copyrighted as indicated in the article. Reuse of AIP content is subject to the terms at: http://scitation.aip.org/termsconditions. Downloaded to IP: 138.253.116.83 On: Thu, 08 May 2014 13:20:35

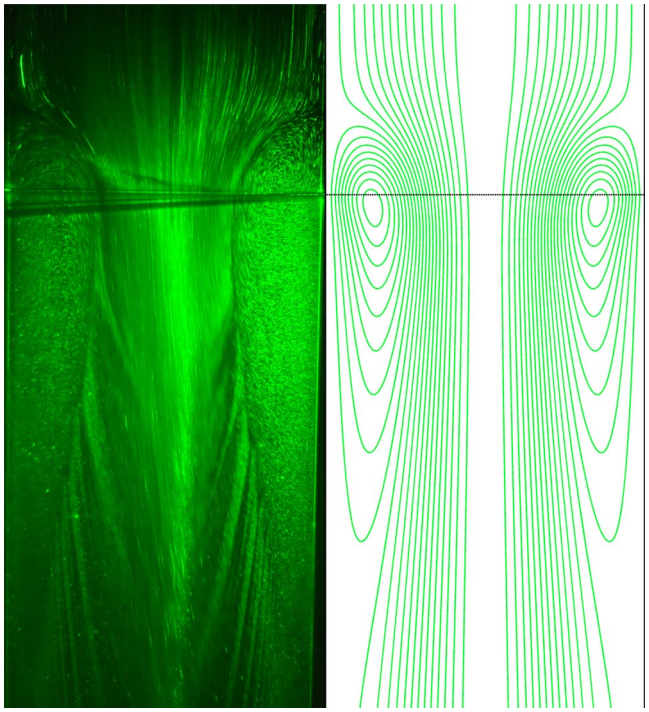

FIG. 7. An illustrative example of vortex breakdown for growing swirl (downstream pipe rotation) $Re = 8$, $\Gamma = 20$; left hand side experiment; right hand side simulation.

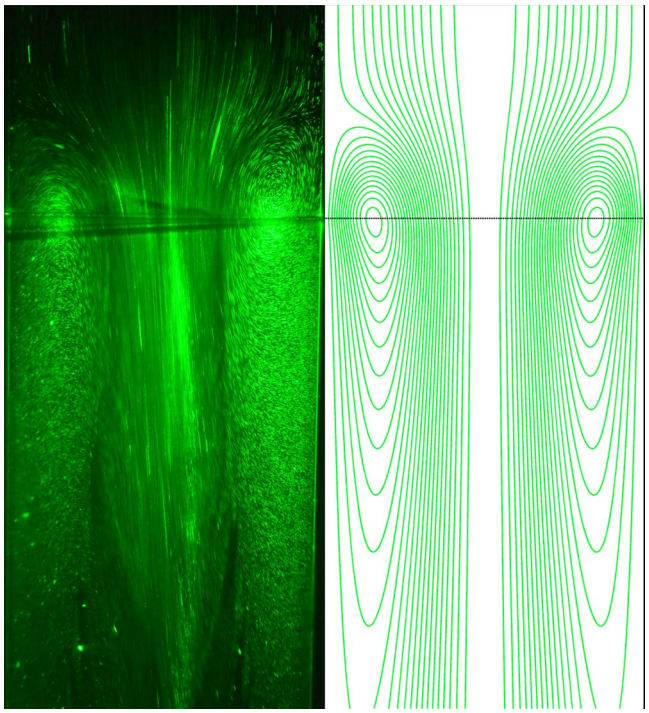

FIG. 8. An illustrative example of vortex breakdown for growing swirl (downstream pipe rotation) $Re = 8$, $\Gamma = 25$; left hand side experiment; right hand side simulation.

This article is copyrighted as indicated in the article. Reuse of AIP content is subject to the terms at: http://scitation.aip.org/termsconditions. Downloaded to IP: 138.253.116.83 On: Thu, 08 May 2014 13:20:35

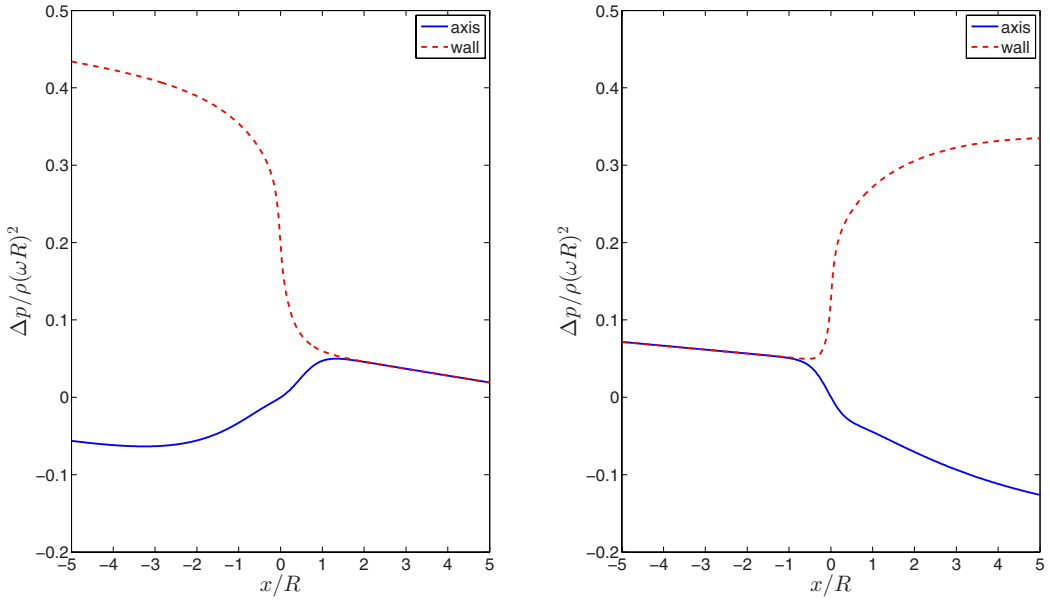

FIG. 9. The axial variation of pressure difference at the wall (dotted line) and axis (solid line) from the numerical simulations using mesh M3. Left hand side decaying swirl (upstream pipe rotation) $Re = 8$, $\Gamma = 15$; right hand side growing swirl (downstream pipe rotation) $Re = 8$, $\Gamma = 20$. The reference pressure ($p = 0$) is the pressure on the pipe axis at the join of the pipes, i.e., at $x/R = r/R = 0$.

the streamlines from the numerical simulation for the equivalent condition. The overall flow pattern is very similar, but it is noted that the centre of the recirculating region appears to be different in the experiment and simulations. In the experiments it is slightly upstream of the pipe join, whereas in the simulations it is just downstream of the join.

The effect of increasing the swirl ratio is demonstrated in Figure 8. The toroidal zone of recirculation grows in both the radial direction (making the "hole" through the centre smaller) and the axial direction. Almost all of this axial growth occurs downstream of the pipe join and the bubble now extends beyond the field of view of the camera (and outside the extent of the optical viewing box). This is significantly longer than any of the decaying swirl cases.

D. The mechanism of flow reversal

Figure 9 shows examples of the axial variation of pressure for decaying and growing swirl, respectively. The plots highlight the difference between the pressure gradient at the pipe wall and axis and demonstrate the key role of the axial pressure gradient in this situation. For decaying swirl the pressure gradient at the wall is favourable ($dp/dx < 0$) and at the axis it is adverse ($dp/dx > 0$). The favourable pressure gradient at the wall leads to an increase in mass flow in the vicinity of the wall with a corresponding decrease near the axis. At sufficiently high swirl ratios the situation is exacerbated to the point at which the mass flow at the axis reaches zero and a stagnation point and subsequently recirculating region is created (effectively reducing the cross-sectional area of the pipe, effectively making it an annulus). For growing swirl the pressure gradients are reversed (favourable at the axis and adverse at the wall) and hence when the swirl ratio is increased above the critical value the flow reversal occurs at the pipe wall and the recirculating region at the wall effectively narrows the pipe, forming an orifice as shown in Figures 7 and 8.

V. CONCLUSIONS AND OUTLOOK

The control of vortex breakdown using wall rotation in pipe flow has been investigated experimentally for the first time and is supported by new numerical simulations. Two cases have been

This article is copyrighted as indicated in the article. Reuse of AIP content is subject to the terms at: http://scitation.aip.org/termsconditions. Downloaded to IP: 138.253.116.83 On: Thu, 08 May 2014 13:20:35

studied: decaying swirl (upstream pipe rotation) and growing swirl (downstream pipe rotation). These two cases create distinctly different flow regimes with the decaying swirl case producing a breakdown bubble on the pipe axis and the growing swirl case causing a toroidal region of recirculation near the wall of the pipe. The flow patterns produced by the axisymmetric simulations are in excellent agreement with those visualised from the experiment. The length of the recirculation region is found to increase radially and axially in extent with increasing Reynolds number and swirl ratio. The extension is particularly apparent in the upstream direction for the decaying swirl case when the swirl ratio is increased. Flow visualisations were used to identify the critical swirl ratio at which the flow undergoes the reversal and vortex breakdown occurs. The prediction of the critical swirl ratio from the numerical simulations is in good agreement with the critical swirl ratio found from flow visualisation. For the decaying swirl case breakdown occurs when $Re\Gamma^2 = 512$ at very low Reynolds numbers (in accordance with an existing analytical solution). At high Reynolds numbers the critical swirl ratio tends to a constant value, $\Gamma = 8$.

The potential future applications of this work include the control of the flow of viscous fluids in pipes, which is a common situation in many industrial settings. Many highly viscous, industrial fluids are non-Newtonian and therefore future work will explore the behaviour of a variety of non-Newtonian fluids in rotating pipe flow. In addition, the interesting case of both pipes rotating simultaneously (either co- or counter-rotating) is to be explored.

ACKNOWLEDGMENTS

The experimental rig used here was designed by Emeritus Professor Marcel Escudier (University of Liverpool) and this significant contribution is hereby gratefully acknowledged. He, in turn, was first alerted to the problem by Dr. Duncan Macdonald (now retired, formerly at University of Liverpool). Some preliminary experiments were conducted by Michael Gobin and Usman Mahmood (both at University of Liverpool) and are also gratefully acknowledged.

[1] D. Peckham and S. Atkinson, "Preliminary results of low speed wind tunnel tests on a gothic wing of aspect ration 1.0," Aeronautical Research Council Technical Report, C.P. No 508, T.N. Aero 2504, 1957.
[2] S. Leibovich, "The structure of vortex breakdown," Ann. Rev. Fluid Mech. **10**, 221–246 (1978).
[3] M. P. Escudier, "Vortex breakdown: Observations and explanations," Prog. Aerospace Sci. **25**, 189–229 (1988).
[4] O. Lucca-Negro and T. O'Doherty, "Vortex breakdown: A review," Prog. Energy Combust. Sci. **27**, 431–481 (2001).
[5] M. Samimy, K. Breuer, L. Leal, and P. Steen, *A Gllery of Fluid Motion* (Cambridge University Press, 2003).
[6] M. P. Escudier, "Observations of the flow produced in a cylindrical container by a rotating endwall," Exp. Fluids **2**, 189–196 (1984).
[7] J. M. Lopez and A. D. Perry, "Axisymmetric vortex breakdown. Part 3. Onset of periodic flow and chaotic advection," J. Fluid Mech. **234**, 449–471 (1992).
[8] M. R. Visbal, "Computed unsteady structure of spiral vortex breakdown on delta wings," AIAA Paper 96-2074, 1996.
[9] M. P. Escudier and N. Zehnder, "Vortex-flow regimes," J. Fluid Mech. **115**, 105–121 (1982).
[10] J. Faler and S. Leibovich, "Disrupted states of vortex flow and vortex breakdown," Phys. Fluids **20**, 1385 (1977).
[11] M. P. Escudier, "Vortex breakdown and the criterion for its occurrence," in *Intense Atmostpheric Vortices*, edited by L. Bengtsson and M. Lighthill (Springer, 1982), pp. 247–258.
[12] Z. Lavan, H. Nielsen, and A. A. Fejer, "Separation and flow reversal in swirling flows in circular ducts," Phys. Fluids **12**, 1747–1757 (1969).
[13] D. Macdonald, "The zeros of $j_1^2(\zeta) - j_0(\zeta)j_2(\zeta) = 0$ with an application to swirling flow in a tube," SIAM J. Appl. Math. **51**, 40–48 (1991).
[14] Z. Rusak and C. Meder, "Near critical swirling flow in a slightly contracting pipe," AIAA J. **42**, 2284–2293 (2004).
[15] C. Crane and D. Burley, "Numerical studies of laminar flow in ducts and pipes," J. Comput. Appl. Math. **2**, 95–111 (1976).
[16] D. Silvester, R. Thatcher, and J. Duthie, "The specification and numerical solution of a benchmark swirling laminar flow problem," Comput. Fluids **12**, 281–292 (1984).
[17] M. P. Escudier, I. W. Gouldson, A. S. Pereira, F. T. Pinho, and R. J. Poole, "On the reproducibility of the rheology of shear-thinning liquids," J. Non-Newtonian Fluid Mech. **97**, 99–124 (2001).
[18] F. Durst, S. Ray, B. Ünsal, and O. Bayoumi, "The development lengths of laminar pipe and channel flows," J. Fluids Eng. **127**, 1154–1160 (2005).
[19] M. P. Escudier, J. OLeary, and R. J. Poole, "Flow produced in a conical container by a rotating endwall," Int. J. Heat Fluid Flow **28**, 1418–1428 (2007).
[20] J. Van Doormaal and G. Raithby, "Enhancements of the simple method for predicting incompressible fluid flows," Numer. Heat Transfer **7**, 147–163 (1984).
[21] J. H. Ferziger and M. Perić, *Computational Methods for Fluid Dynamics*, Corr. 2nd print ed. (Springer, Berlin, 1997).

This article is copyrighted as indicated in the article. Reuse of AIP content is subject to the terms at: http://scitation.aip.org/termsconditions. Downloaded to IP: 138.253.116.83 On: Thu, 08 May 2014 13:20:35